Figure S1. Combination treatment with RCM-1 and venetocalx impairs cell viability and induces apoptosis *in vitro*: (A) Dose-response curves to determine the IC_{50} of RCM-1 and venetoclax. Left panels, human fusion-negative RMS cell line (RD). Right panels, murine RMS cell line (76-9). (B) The results of the CCK8 assay showed a significant decrease in cell viability following RCM-1 and venetocalx in RD, 76-9 and (C, left panel) RH30 RMS cells. (C, right panel) Significant increase in caspase 3/7 activity after RCM-1 and venetoclax treatment $^{*}P\leq0.05$, $^{**}P\leq0.01$, $^{***}P\leq0.001$, $^{****}P\leq0.0001$. RMS, rhabdomyosarcoma; IC_{50}, 50% inhibitory concentrations.

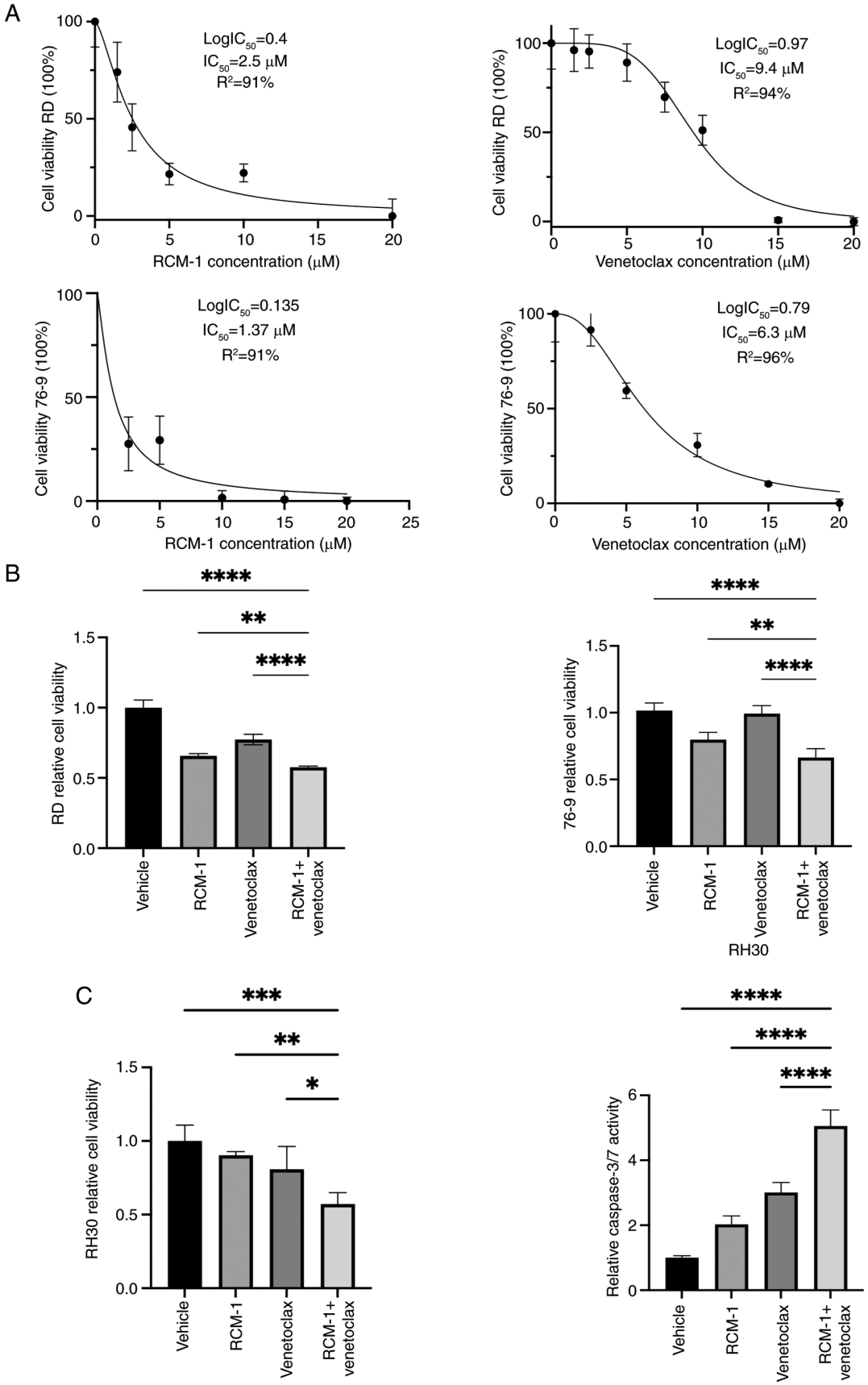

Figure S2. Safety profile of RCM-1 and venetoclax combination therapy in a mouse model of RMS. (A) No significant change in mice weight treated with the combination therapy compared with single agents and control. (B) The combination therapy was safe and well tolerated in mice. A significant decrease in white blood cell counts in venetoclax-treated mice compared with control and RCM-1-treated mice. (C) No liver toxicity was detected in the treatment groups. **P≤0.01, ***P≤0.001. RMS, rhabdomyosarcoma; ALT, Alanine Aminotransferase; AST, Aspartate Aminotransferase.

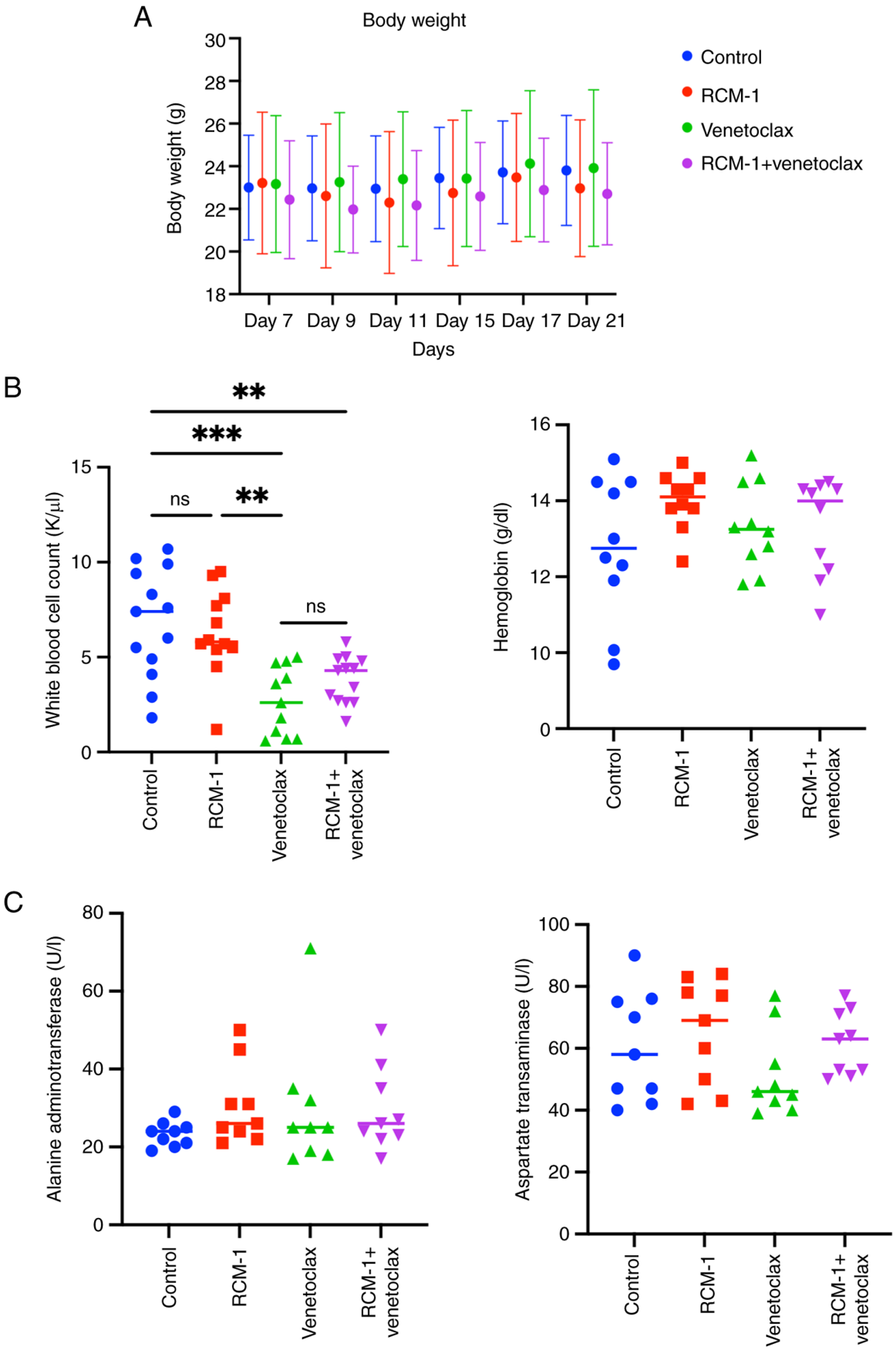

Figure S3. scRNA-seq analysis from human muscle tissue identifies SMC, skeletal muscle and myoblast cell populations. (A) UMAP showed the skeletal muscle cell clusters from 10 healthy human donors (GSE143704 dataset) and the violin plots of expression levels from well-known marker genes in each cell type (ACTA2 for smooth muscle cells, ACTA1 for skeletal muscle cells and PAX7 for myoblasts), color-coded by the identified subpopulations. (B) Violin plots of expression level showed the antiapoptotic gene, Bcl2 and the cell cycle inhibitor gene, CDKN1A, in each cell type, color-coded by the identified subpopulations. SMC, smooth muscle cells; UMAP, Uniform Manifold Approximation and Projection.

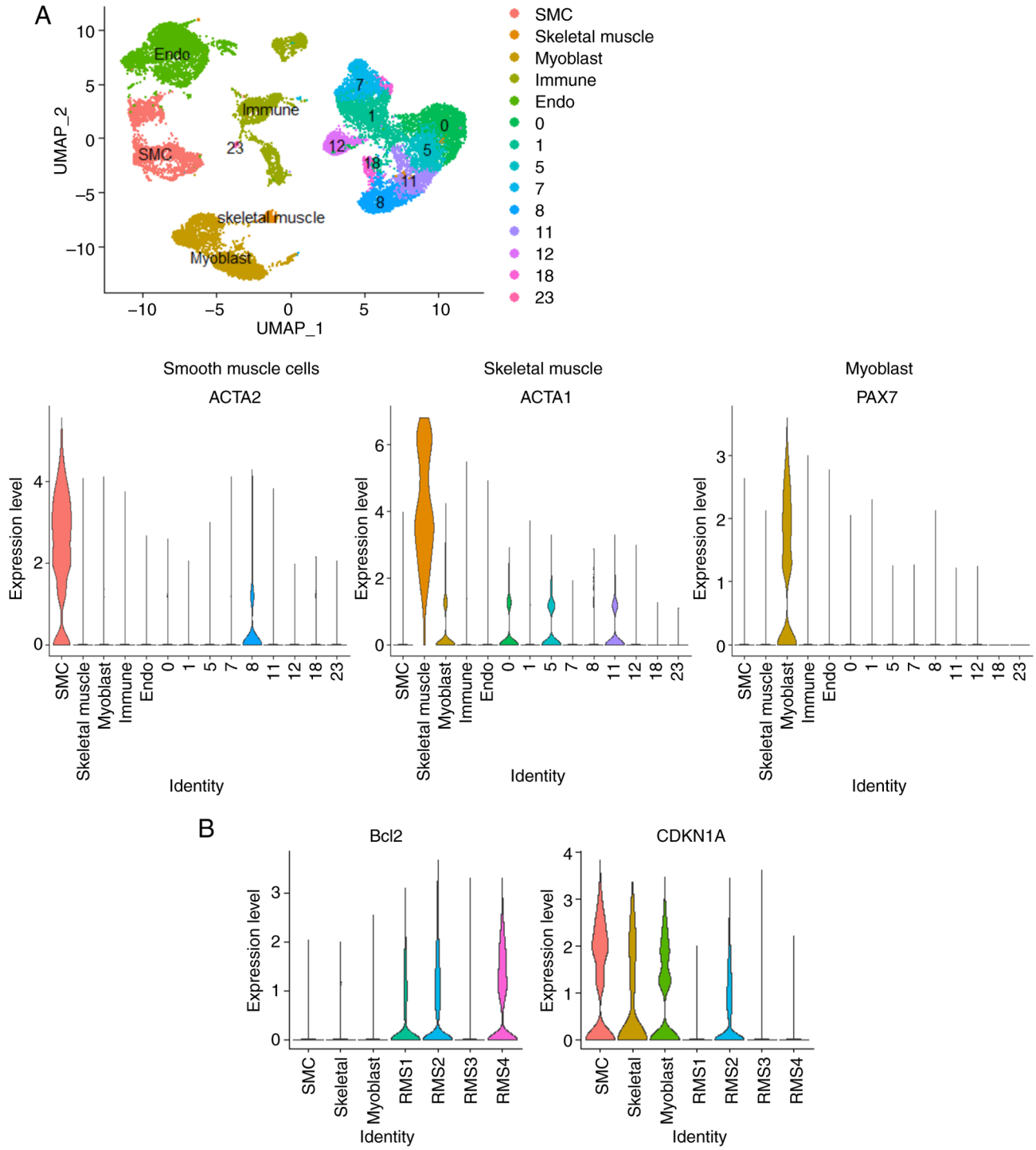

Figure S4. Transfection efficiency in 76-9 RMS cells. (A) 76-9 cells were transfected with SMARTpool against siATP2B4 or non-targeting siRNA. Left panel, the knockdown efficiency of siATP2B4 measured by RT-qPCR. *Actb* mRNA was used for normalization. The knockdown resulted in ~45% decrease in *Atp2b4* mRNA level after 24 h and about 87% reduction after 48 h of transfection. Right panel, immunofluorescence staining showed decreased protein levels of ATP2B4 in siATP2B4 76-9 cells. (B) 76-9 cells were transfected with empty plasmid OE, CMV-ATP2B4a, or CMV-ATP2B4b. Left panel, analysis of overexpression efficiency by RT-qPCR. *Actb* mRNA was used for normalization. Right panel, immunofluorescence staining showed increased protein levels of ATP2B4 in mATP2B4a/b overexpressed 76-9 cells. *P≤0.05, **P≤0.01, ***P≤0.001, ****P≤0.0001. RMS, rhabdomyosarcoma; si, small interfering; RT-qPCR, reverse transcription-quantitative PCR; OE, overexpression.

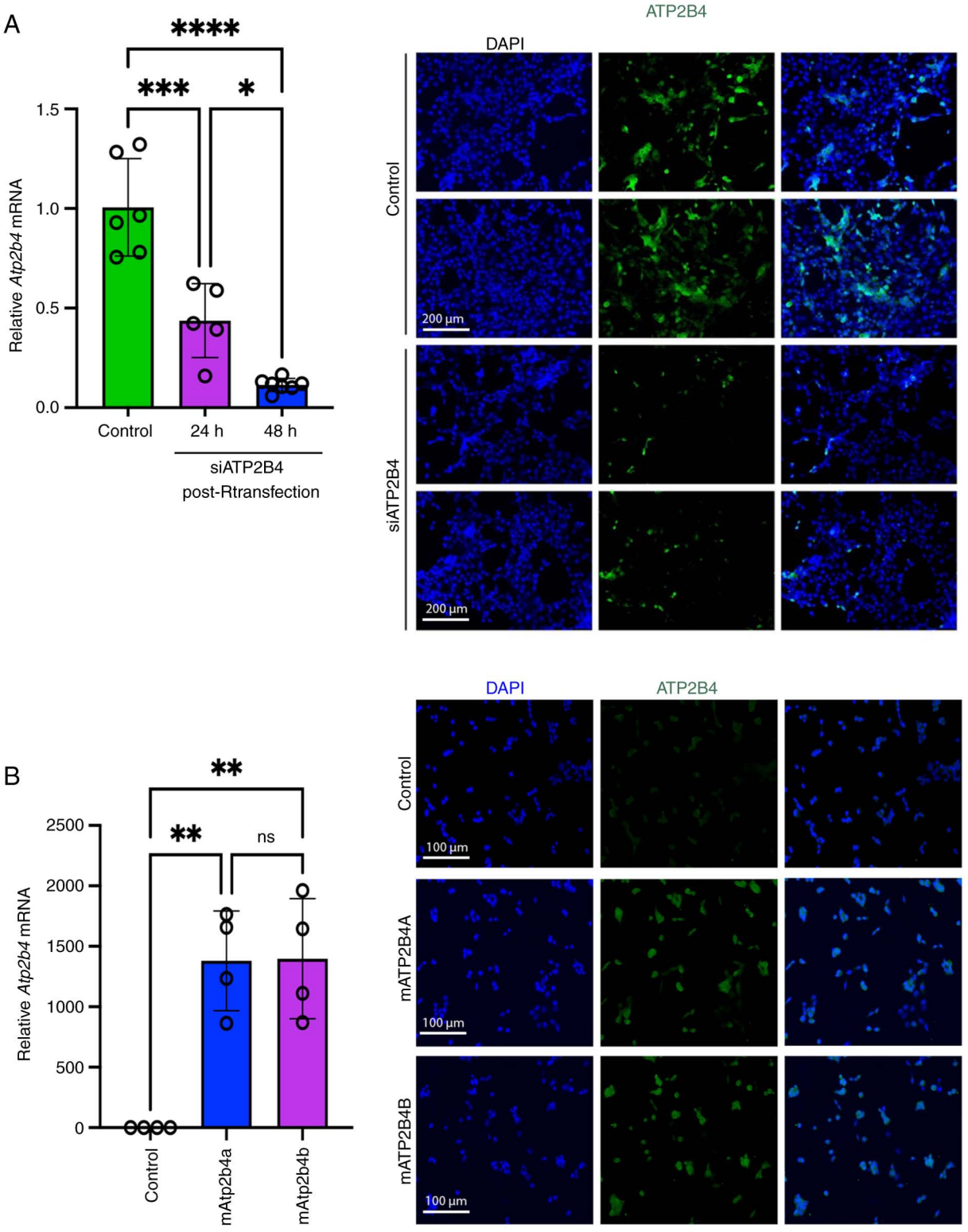

Figure S5. Transduction efficiency of shAtp2b4 in 76-9 cells. (A) Knockdown efficiency of shAtp2b4 measured by reverse transcription-quantitative PCR in 76-9 cells. *Actb* mRNA was used for normalization. shAtp2b4 resulted in a significant reduction in ATP2B4 mRNA levels compared with control. (B) Immunofluorescence staining of tumor sections showed decreased protein levels of ATP2B4 in shAtp2b4 tumors. ***P≤0.001, ****P≤0.0001. sh, short hairpin.

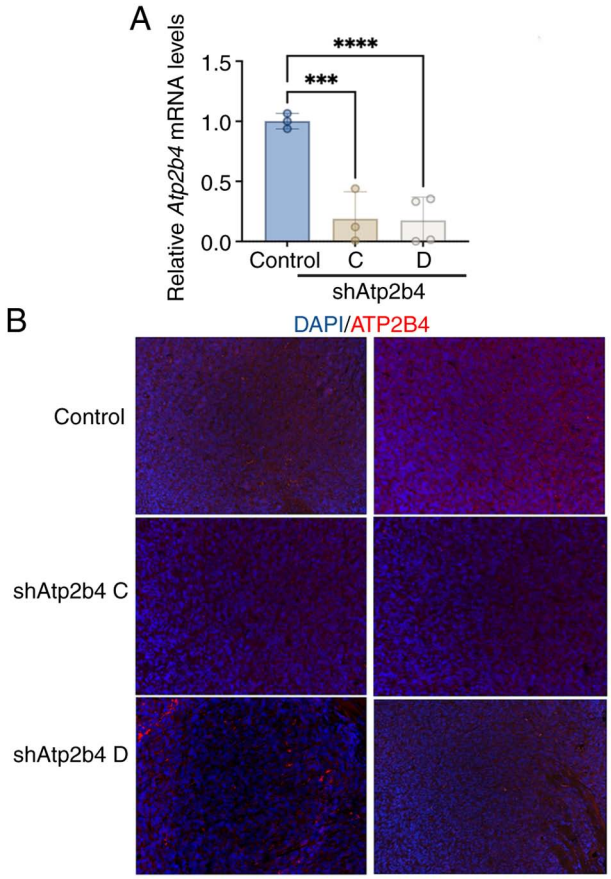

Figure S6. (A) Analysis of *Foxm1* overexpression efficiency by reverse transcription-quantitative PCR. *Actb* mRNA was used for normalization. (B) Gross and unedited images of control and shAtp2b4 RMS tumors. ***P≤0.001. sh, short hairpin; RMS, rhabdomyosarcoma.